Materials Science and Engineering B 174 (2010) 18–30

Contents lists available at ScienceDirect

Materials Science and Engineering B

journal homepage: www.elsevier.com/locate/mseb

Review

Sol–gel-deposited ZnO thin films: A review

Lamia Znaidi*

Laboratoire d'Ingénierie des Matériaux et des Hautes Pressions (LIMHP), CNRS-UPR 1311, Université Paris 13, 99 Avenue J.B. Clément, 93430 Villetaneuse, France

ARTICLE INFO

Article history:
Received 31 August 2009
Received in revised form 6 June 2010
Accepted 3 July 2010

Keywords:
Zinc oxide
Sol–gel
Colloids
Thin films
Preferential orientation
c-Axis

ABSTRACT

During the last years, ZnO thin films have been studied extensively due to their potential applications in e.g. piezoelectric and optoelectronic devices or photovoltaic cells. Ordered *c*-axis orientation of ZnO crystallites is desirable for applications where crystallographic anisotropy is a prerequisite such as for short-wavelength semiconductor diode lasers (SDLs), and piezoelectric surface acoustic wave or acousto-optic devices. Many works were dedicated to *c*-axis oriented ZnO thin films elaboration and the study of their properties, including physical and chemical methods. For instance, sol–gel processes are particularly well adapted to produce ZnO films in a simple, low-cost and highly controlled way. This review summarizes the main chemical routes used in the sol–gel synthesis of undoped ZnO thin films and highlights the chemical and physical parameters influencing their structural properties. In this process, the ZnO films synthesis includes three principal steps: (i) solution preparation, (ii) coating and (iii) heat treatment. For the first step, the particle formation is discussed including nucleation and growth, particle size, morphology and colloids stability. These three steps involve several parameters such as: (i) nature and concentration of precursor, solvent and additive, and solution aging time, for the chemical system, (ii) coating method, thickness and substrate for the coating step, and (iii) pre-and post-heat treatment for the last step. The influence of these steps and synthesis parameters on ZnO thin films orientation is discussed.

Contents

* Tel.: +33 1 49 40 34 45; fax: +33 1 49 40 34 14.
E-mail address: lamia@limhp.univ-paris13.fr.

0921-5107/$ – see front matter © 2010 Elsevier B.V. All rights reserved.
doi:10.1016/j.mseb.2010.07.001

1. Introduction

During the last years, ZnO thin films have been studied extensively due to their potential applications, as piezoelectric transducers, optical waveguides, acousto-optic media, surface acoustic wave devices, conductive gas sensors, transparent conductive electrodes, solar cell windows, and varistors [1–4].

ZnO, a II–VI semiconductor, is now recognized as a promising candidate for blue and ultraviolet light-emitting diodes or laser diodes because of its wide-band gap of 3.37 eV and large exciton binding energy of 60 meV [2–7]. Its large exciton binding energy allows excitonic absorption and recombination even at room temperature, which makes this material appealing [7]. Excitonic laser oscillation with a very low threshold (24 kW/cm^2) at room temperature was confirmed in 50 nm thin films on sapphire (0 0 0 1) substrates [7]. Such observations indicate that an exciton-related recombination process can be utilized as an optoelectronic device operable at room temperature [7].

Reynolds et al. [8] published in 1996 the first report of optically pumped lasing at low temperature (2 K) from a ZnO platelet grown from the vapor phase. One year later, ultraviolet spontaneous and stimulated emissions from ZnO thin films at room temperature were observed by Zu et al. [9], Bagnall et al. [10] and Segawa et al. [11]. These studies were followed by the works by Bagnall et al. [12], Yu et al. [13], Tang et al. [14], Kawasaki et al. [15] and Ohtomo et al. [16] in 1998. In these studies, ZnO thin films were principally elaborated by laser molecular-beam epitaxy (L-MBE), showing high crystallinity with *c*-axis orientation (*c*-axis perpendicular to the substrate). These films consist of an epitaxially ordered array of hexagonal microcrystallites; and the facets of all hexagons are parallel to those of the others, forming natural Fabry–Pérot lasing cavities [13,14]. The grain size in these films is about 50–55 nm in most cases; and the film thicknesses lie between 50 and 500 nm. Yu et al. [13] reported room temperature measurements of optical gain and gain spectra of ultraviolet emission from ZnO thin films. They found that the lasing threshold has a minimum near a film thickness of 55 nm; increasing rapidly for films with thickness of 40 nm; and no lasing was observed in films thinner than 30 nm. Kawasaki et al. [15] reported that there is an optimum crystallite size of 50 nm for observing excitonic stimulated emission.

On the other hand, the orientation along the *c*-axis parallel to the substrate surface was also observed in the case of epitaxial ZnO and group-III-nitride thin films [17–19]. Lin et al. [17] have prepared epitaxial ZnO films by metal-organic chemical vapor deposition (MOCVD) on γ-$LiAlO_2$ substrate. The authors reported that the polarized Raman and optical transmission spectra indicated that these epitaxial films exhibited optical anisotropy, which have applications in certain optical devices, such as the UV modulator and polarization-dependent beam switch. Also, Wraback et al. [18] used the same method (MOCVD) for preparing epitaxial ZnO films on the (0 1 $\bar{1}$ 2) surface of sapphire substrates. They have demonstrated an optically addressed normal incidence ultraviolet light modulator, which exploits the optical anisotropy inherent in ZnO epitaxially grown on (0 1 $\bar{1}$ 2) sapphire to achieve high contrast. They reported that such films are interesting for acousto-optic, photochromic, and piezoelectric device applications. Schaadt et al. [19] have used the molecular-beam epitaxy for preparing the group-III-nitride thin films (GaN/AlN) grown on γ-$LiAlO_2$ by molecular-beam epitaxy. The authors presented a polarization-dependent beam switch based on group-III-nitride thin films and they have fabricated a two-color distributed Bragg reflector consisting of alternating (1 $\bar{1}$ 0 0)-oriented (M-plane) AlN and GaN layers. They have demonstrated that this birefringent distributed Bragg reflector offers two main functionalities, polarization-dependent beam switching and polarization selection. They reported that group-III nitrides of the wurtzite crystal structure exhibit linear birefringence (the refractive index is different for light polarized parallel and perpendicular to the *c*-axis) and in films grown on non-polar surfaces, where the *c*-axis lies in the film plane, this effect can be utilized for beam switching and polarization selection.

Besides, Romero et al. [20] reported that in order to be properly suitable for acoustic wave devices, polycrystalline ZnO thin films must meet two requirements. First, the basal plane of ZnO crystallites must be oriented parallel to the plane of the substrate (*c*-axis orientation). Second, the ZnO thin films must have a columnar structure with void-free grain boundaries. For these reasons, *c*-axis oriented thin ZnO thin films are of interest for the production of surface and bulk acoustic wave devices. The tilt of the *c*-axis can determine the type of ultrasonic wave produced by pulse-echo transducers [20]. Martin et al. [21] have deposited piezoelectric ZnO thin films by reactive magnetron sputtering for use in ultrasonic transducers. They reported that the films with the optimum piezoelectric response were achieved in transducers that possessed the hexagonal (0 0 2) crystal orientation. The tilt of the *c*-axis determined the type of ultrasonic wave produced by the pulse-echo transducers. When the angle of the *c*-axis to the substrate surface was 0°, the longitudinal mode (L-wave) was dominant. At a 16° tilt, the longitudinal and shear waves (S-wave) were mixed, and at a tilt of 41°, the shear wave was dominant [21].

So, the both orientation (*c*-axis perpendicular or parallel to the substrate) were observed in ZnO thin films. Nevertheless, the *c*-axis perpendicular to the substrate stays the one, which is mostly observed and especially when the growth is not made by epitaxy. This point will be discussed in Section 3.2. In the following text, *c*-axis or (0 0 2) orientation means *c*-axis perpendicular to the substrate; and *a*-axis or (1 0 0) orientation means *c*-axis parallel to the substrate.

In brief, ZnO crystallites with preferential orientation are desirables for applications where crystallographic anisotropy is a prerequisite such as for UV diode lasers [9–18], and piezoelectric surface acoustic wave or acousto-optic devices [3,5,19–21].

A lot of methods have been extensively used for oriented ZnO films synthesis, including L-MBE, pulsed laser deposition, metal-organic chemical vapor deposition, sputtering [2], cathodic magnetron sputtering and reactive electron beam evaporation [21–25], spray pyrolysis [20,26–28], and electrodeposition [29,30]. However, sol–gel processes are particularly adapted to produce ZnO colloids [31–42] and films [4,43–49] in a simple, low-cost and highly controlled way.

The sol–gel process, called also soft chemistry ('chimie douce'), allows elaborating a solid material from a solution by using a sol or a gel as an intermediate step (Scheme 1), and at much lower temperatures than is possible by traditional methods of preparation. It enables the powderless processing of glasses and ceramics, and thin films or fibers directly from solution. The synthesis of solid materials via 'chimie douce' often involves wet chemistry reactions and sol–gel chemistry based on the transformation of molecular precursors into an oxide network by hydrolysis and condensation reactions [50,51].

Scheme 1 shows the main steps of preparation of thin films and powder by the sol–gel process. We can summarize, for example, the film preparation in three parts: (i) preparation of the precursor solution; (ii) deposit of the prepared sol on the substrate by the chosen technique; and (iii) heat treatment of the xerogel film. The xerogel is the dried gel at ambient pressure (the dried gel in supercritical conditions is called aerogel).

The detail of these steps and the process parameters will be discussed in the following sections.

The objective of this review is to summarize the main chemical routes used in the sol–gel synthesis of undoped ZnO thin films and to highlight the chemical and physical parameters influencing their structural properties. ZnO thin film synthesis involves several

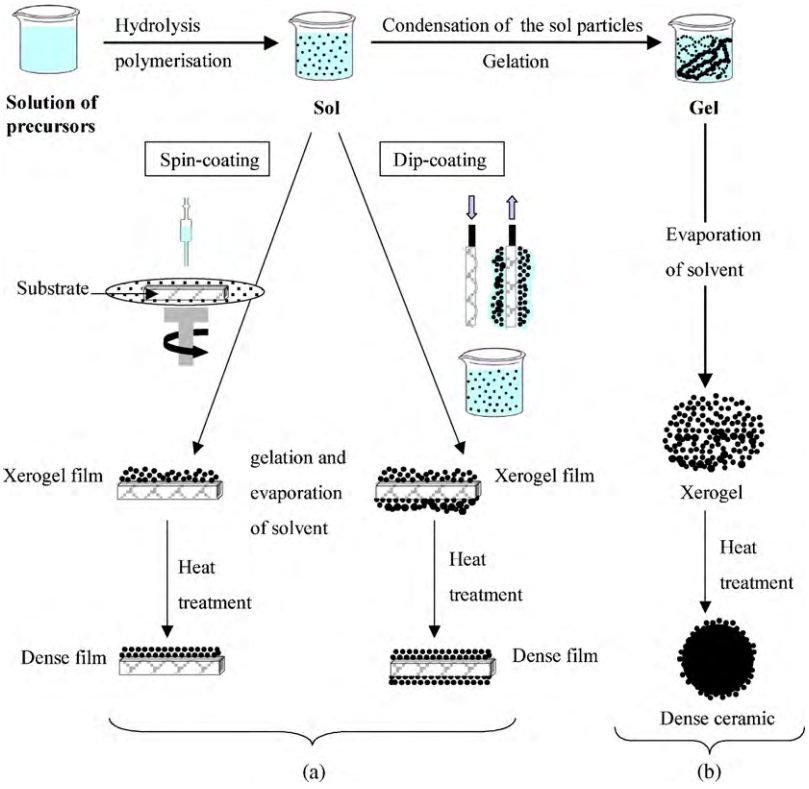

Scheme 1. Overview showing two synthesis examples by the sol–gel method; (a) films from a colloidal sol; (b) powder from a colloidal sol transformed into a gel.

parameters: (1) the nature of the precursor and its concentration, (2) the type of solvent and the acidity of the medium, (3) the type of additive species and their concentrations, (4) the aging time of the early mixture, (5) the method of coating of substrates and its speed, (6) the nature of the substrate, and (7) the pre- and post-heat treatment of the materials. A survey of the literature shows that all these parameters play a key role on the evolution of texture in zinc oxide films.

First of all, it should be noted that several works led to significantly different results particularly concerning the crystallographic orientation even if the experimental conditions were very close to each other. This makes difficult any prediction or any clear correlation. Thus the aim of this paper is to underline the main principles that emerge for each parameter and have a great influence on the elaboration of crystallized and textured zinc oxide films.

2. Sol–gel method toward zinc oxide synthesis

2.1. Chemical systems: precursors, solvents, and additives

In the sol–gel process, a molecular precursor in a homogeneous solution undergoes a succession of transformations: (a) hydrolysis of the molecular precursor; (b) polymerization via successive bimolecular additions of ions, forming oxo-, hydroxyl, or aqua-bridges; (c) condensation by dehydration; (d) nucleation; and (e) growth [52,53]. Depending on the nature of the molecular precursors, two sol–gel routes are currently used: metal alkoxides in organic solvents or metal salts in aqueous solutions [50]. The main methods of ZnO film elaboration, as reported in the literature, involve several steps and are in fact intermediate between the two sol–gel methods since they use metal salts in alcoholic solutions. Indeed, ZnO films are obtained starting from inorganic salts – nitrates, chlorides, perchlorates – or organic salts like acetates and acetylacetonates, dissolved in alcoholic media. It is believed that in such media the process involves two steps. The first one consists of *in situ* formation of alkoxide or alkoxy-complexes. In the second step, these complexes undergo transformation through hydrolysis and polymerization to lead to the oxide.

Table 1 summarizes the sol–gel undoped ZnO thin film elaboration methods including chemical systems used and results concerning crystallographic orientation.

2.1.1. Precursors

Several zinc precursors have been used: nitrate, chloride, perchlorate, acetylacetonate and alkoxides such as ethoxide and propoxide, but the most often used is the acetate dehydrate. Metal alkoxides, although they offer several chemical advantages, are not suitable because they are very sensitive to moisture, highly reactive and remain still rather expensive. Because of their low cost, facility of use, and commercial availability, metal salts are interesting as precursors and could be more appropriate for large-scale applications. Since metal salts include inorganic and organics ones, we can underline the comparisons made between them and reported by some authors. Inorganic salts like nitrates are often used, as precursors for sol–gel ZnO-based materials, even though their main drawback is related to the inclusion or difficult removal of anionic species in the final product [51,54]. Using zinc acetate as a precursor, the acetate groups, as contaminants of the gel, decompose under annealing producing combustion volatile by-products [54]. Bahnemann et al. [33] synthesized transparent colloidal suspensions of zinc oxide in water, 2-propanol, acetonitrile, and using different zinc salts. They reported that the anion, in zinc salt, is critical for the preparation of transparent and stable ZnO colloids. They mentioned that the use of zinc perchlorate instead of zinc acetate yields a turbid suspension; i.e., coagulation of the particles takes place, the acetate acts so as stabilizer of the colloidal sol. Also, the experiments with $ZnCl_2$ or $Zn(NO_3)_2$ reveal a faster coagulation than in the case of $Zn(ClO_4)_2$ following the initial formation of a

Table 1
Main chemical systems used for undoped ZnO thin films elaboration by sol–gel process in alcoholic medium and resulting film crystallographic orientation.

References	Precursor ($mol\,L^{-1}$)	Alcohol	Additive (r)	H_2O (h)	Aging time	Substrate	Pre-heat treatment (°C)	Post-heat treatment (°C)	Thickness (nm)	Crystallographic orientation
Natsume and Sakata [61]	ZAD (0.02)	MeOH	–	–	–	Pyrex	80	500–575	160–230	(002)
González et al. [62]	ZAD (0.59)	MeOH	–	–	24 h	Corning glass	50	300, 450 150	35–204	(100) **(002)** (101) **(100)** (002) (101)
Santos et al. [63,64]	ZAD[a]	MeOH	–	–	–	Glass	120	350	(18L)[a]	(002)
Sagar et al. [65,66]	ZAD (0.6)	MeOH	MEA (0–1)	–	48 h	Corning glass	300	400–600	180–190	(002)
Liu et al. [67,68]	ZAD (0.6)	EtOH, PEG (14 g/L)	DEA (1)	(2)	–	Glass	100	500	220 (6L)	(100) (002) **(101)**
Wang et al. [69]	ZAD (0.5)	EtOH	DEA (1)	–	–	Quartz	400	400–800	300 (6L)	(100) (002) **(101)**
Kumar et al. [70]	ZAD (0.2)	EtOH	DEA (1)	–	48 h	p-Si(100)	250	350–450	~250	(100) **(002)** (101)
Shaoqiang et al. [4]	ZAD (0.46)	EtOH	–	–	–	n- and p-type Silicon	40	500 (directly)	200	(002)
								500 (Gradually)		(100) **(002)** (101)
Znaidi et al. [47,48]	ZAD (0.05)	EtOH	MEA (2)	–	72 h	Glass	100–135	450	–	(100)
Wang et al. [71]	ZAD (1.8)	EtOH	MEA (1.5)	–	72 h	Glass	300	350–600	(5L)[a]	(100) **(002)** (101)
Wang et al. [72]	ZAD (0.19)	EtOH	Ac. Ac. (0.35)	(11.1)	24 h 2 h	Glass	100	450	–	(100) Amorphous film
Bao et al. [46]	ZAD (0.4)	EtOH	Lactic Ac.	–	–	Quartz	300	500, 550 450, 600	300 (6L)	(002) (100) **(002)** (101)
Bole and Patil [73]	ZAD[a]	EtOH	Lactic Ac.	–	–	Glass	300	300–425	375–275	**(100)** (002) (101)
Kavanagh and Cameron [74]	ZAD[a]	EtOH	Lactic Ac.	(2)	–	Silicon	240	700	–	(100) **(002)** (101)
Bahadur and Rao [75]	ZAD[a]	EtOH	$LiOH{\cdot}H_2O$	–	–	F:SnO_2	80	400	800 (5L)	(100) (002) **(101)**
Brenier and Ortéga [76]	ZAD (0.15)	1-PrOH	TMAH	–	4 weeks	Silicon	80	250 (O_2)	20–60	(100) (002) **(101)**
Peterson et al. [77]	ZAD (0.3)	1-PrOH	Glycerol	–	–	Si(100), quartz	300	700	180 (4L)	(100) **(002)** (101)
Raoufi et al. [78]	ZAD (0.3)	1-PrOH	MEA (1)	–	–	Glass	250	300–500	500 (8L)	(100) **(002)** (101)
O'Brien et al. [79] and Rao et al. [80]	ZAD (0.3–0.7) (1.3)	2-PrOH	MEA (1)	–	24 h	UV fused silica	60	450–650	84–437	(100) **(002)** (101) (100) (002) **(101)**
Kim et al. [3]	ZAD (0.3–0.5) (0.7) (1–1.3)	2-PrOH	MEA (1)	–	24 h	Corning glass	250	650	–	Amorphous film (100) **(002)** (101) (100) (002) (101)[b]
Lin and Kim [81]	ZAD (0.5)	2-PrOH	DEA (1)	–	24 h	Si(100), Glass	300	450–550	280 (7L)	(100) (002) (101)[b]
						Si(100)		700, 800		(100) **(002)** (101)
Aslan et al. [82]	ZAD (0.4)	2-PrOH	DEA (1)	(0.5)	–	Glass	250	450–550	1000–1600 (10–15L)	(100) **(002)** (101)
Chakrabarti et al. [83]	ZAD (0.24)	2-PrOH	DEA (0.006)	–	–	Glass p-Si(100), Soda-lime, quartz, alumina	100	550 700	–	(002) (100) **(002)** (101)
Jiwei et al. [84]	ZAD (0.4)	2-PrOH	DEA (1)	(2)	–	SiO_2/Si(111), fused-quartz	200 (O_2)	300–650 (O_2)	230–350	(100) **(002)** (101)
Wang et al. [85]	ZAD (0.32)	2-PrOH	DEA (1)	–	–	Si/SiO_2/Ti/Pt	300–450	550–800	500 (6L)	(100) **(002)** (101)
Bae and Choi [86]	ZAD (0.25)	2-PrOH	DEA (1.5)	–	–	Alumina	300	400–900	125–240 (3–6L)	(100) (002) (101)[b]
Ohya et al. [44,87] and Takahashi et al. [88]	ZAD (0.25/0.5)	2-PrOH	DEA (1)	(2)	–	Glass	110	350–600	13–33/L	(100) **(002)** (101)
Mridha and Basak [89]	ZAD (0.1)	2-PrOH	DEA	–	–	Glass	120	550	260	(100) **(002)** (101)
Dutta et al. [90]	ZAD (0.03–0.1)	2-PrOH	DEA	–	–	Glass	350	550	36–247	(100) (002) **(101)**
Basak et al. [91]	ZAD (0.6)	2-PrOH	DMA	–	–	Sapphire	120	550	300 (10L)	(100) **(002)** (101)
Ghosh et al. [6,92,93]	ZAD (0.6)	2-PrOH	DMA	–	–	Quartz Glass, Si/SiO_2 GaN	120	550	400 (10L)	(100) (002) **(101)** (100) **(002)** (101) (002)
Zhang et al. [94]	ZAD (0.3)	PVA	–	–	–	Si(100)	120	600	434	(100) **(002)** (101)
Pal and Sharon [95]	ZA (<0.03)	2-PrOH	NaOH (1)	–	–	Glass	–	400	(5–6L)[a]	(100) (002) **(101)**
Abdel Aal et al. [96]	ZAD[a]	2-PrOH	NaOH	–	–	Glass	–	550	(6L)[a]	(002)
Caglar et al. [97]	ZAD (1)	2-ME	MEA (1)	–	–	p-type single crystal Si	300, 450	550–750	(10L)[a]	(100) **(002)** (101)
Ohyama et al. [98]	ZAD (0.75)	2-ME	MEA (1)	–	–	Silica	300	600	100–260	(002)
Li et al. [99,100]	ZAD (0.75)	2-ME	MEA (1)	–	–	Silica	300	600	300 (7L)	(002)
Zhu et al. [101]	ZAD (0.75)	2-ME	MEA (1)	–	–	Glass	60	400–550	(4L)[a]	(100) **(002)** (101)
Fujihara et al. [102]	ZAD (0.75)	2-ME	MEA (1.1)	–	–	Glass	400–500	400–500	200 (5L)	(002)
Znaidi et al. [47,48]	ZAD (0.75)	2-ME	MEA (2)	–	–	Glass	300	500–550	76 (3L)	(002)
Ohyama et al. [45]	ZAD (0.6)	2-ME	MEA (1) DEA (1)	–	–	Silica	500	500	–	(002) (100) (002) (101)[b]
Nagase et al. [103]	ZAD (0.6)	2-ME	MEA (1)	–	–	Quartz	200	Laser irradiation	35–190	(002)
Hsieh et al. [104,105]	ZAD (0.6)	2-ME	MEA (1)	–	–	SiO_2/Si	270	600–900	–	(100) **(002)** (101)
Yoon et al. [106]	ZAD (0.5)	2-ME	MEA (1)	–	72 h	SiN_x/Si, Pt(111)/Si	300	700	140 (5L)	(002)

Table 1 (*Continued*)

References	Precursor (mol L^{-1})	Alcohol	Additive (r)	H_2O (h)	Aging time	Substrate	Pre-heat treatment (°C)	Post-heat treatment (°C)	Thickness (nm)	Crystallographic orientation
			DEA (1)			SiN_x/Si,				(1 0 0) (0 0 2) (1 0 1)[b]
			DEA (1)			Pt(1 1 1)/Si				(0 0 2)
Choi et al. [107]	ZAD (0.5)	2-ME	MEA (1)	–	–	Pt/TiO_2/SiO_2/Si	300	400–700	180	(0 0 2)
Srinivasan et al. [108–110]	ZAD (0.5)	2-ME	MEA (1)	–	–	Glass, quartz	350	500	(8L)[a]	(1 0 0) **(0 0 2)** (1 0 1)
						(0 0 1) sapphire	100, 400	450–600	530 (10L)	(1 0 0) **(0 0 2)** (1 0 1)
Kokubun et al. [111]	ZAD (0.45)	2-ME	MEA (1)	–	–	Silica	90/300	500/600	150	(1 0 0) **(0 0 2)** (1 0 1)
Lee et al. [112]	ZAD (0.35)	2-ME	MEA (1)	–	48 h	Corning glass	350	600	200	(0 0 2)
Xue et al. [113]	ZAD (0.35)	2-ME	MEA (1)	–	24 h	Fused silica	300	500	800 (12L)	(1 0 0) **(0 0 2)** (1 0 1)
Castanedo-Pérez et al. [114]	ZAD (1.14)	EG, 1-PrOH	Glycerol, TEA	(0.31)	30 h	Soda-lime glass, silicon	100	450	160	(1 0 0) (0 0 2) **(1 0 1)**
Delgado et al. [115]	ZAD[a]	EG, 1-PrOH	Glycerol, TEA	–	24 h	Glass	100	200–600	450 (5L)	(1 0 0) (0 0 2) **(1 0 1)**
Kamalasanan and Chandra [116]	ZAD (<1.98)	EG, 1-PrOH	Glycerol, TEA	–	–	Soda glass, silicon	–	450	200/L	(1 0 0) **(0 0 2)** (1 0 1)
Chatterjee et al. [117]	ZNH[a]	PVA	–		–	Silicon	–	700–850	∼1000	(1 0 0) **(0 0 2)** (1 0 1)
Toyoda et al. [118]	ZNH[a]	2-ME	–	–	–	Platinized Si	25	250–450	[a]	(0 0 2)
								600		(1 0 0) (0 0 2) **(1 0 1)**
Okamura et al. [43,119]	$Zn(OEt)_2$[a]	1-BuOH	Acac	–	–	p-Si(1 1 1)	–	700 (O_2)	20/L	(1 0 0) (0 0 2) (1 0 1)[b]
Ohya et al. [44,87]	$Zn(OPr^n)_2$ (0.2/0.5)	2-PrOH	DEA (1)	(2)	–	Glass	110	600	11–33/L	(1 0 0) **(0 0 2)** (1 0 1)

Abbreviations (Abbrev.):

Abbrev.	Product name	Chemical formula	Abbrev.	Product name	Chemical formula
ZAD	Zinc acetate dihydrate	$[Zn(CH_3COO)_2{\cdot}2H_2O]$	MeOH	Methanol	CH_3OH
ZA	Zinc acetate anhydrous	$[Zn(CH_3COO)_2]$	EtOH	Ethanol	C_2H_5OH
ZNH	Zinc nitrate hexahydrate	$[Zn(NO_3)_2{\cdot}6H_2O]$	1-PrOH	1-Propanol	C_3H_7OH
MEA	Monoethanolamine	$(HOCH_2CH_2)NH_2$	2-PrOH	2-Propanol	$(CH_3)_2CHOH$
DEA	Diethanolamine	$(HOCH_2CH_2)_2NH$	1-BuOH	1-Buthanol	C_4H_9OH
TEA	Triethanolamine	$(HOCH_2CH_2)_3N$	2-ME	2-Methoxyethanol	$CH_3O(CH_2)_2OH$
DMA	Dimethylamine	$(CH_3)_2NH$	EG	Ethylene glycol	$HO(CH_2)_2OH$
PVA	Polyvinyl alcohol	$[-CH_2CH(OH)-]_n$	PEG	Polyethylene glycol	$H(OCH_2CH_2)_nOH$
TMAH	Tetramethylammonium hydroxide	$(CH_3)_4N(OH)$	Ac. Ac.	Acetic Acid	CH_3COOH
Acac	Acetylacetone	$CH_3COCH_2COCH_3$	Lactic Ac.	Lactic Acid	$CH_3CHOHCOOH$

In the thickness column: L: layer. The numbers between brackets for additive and water columns correspond to r and h values, respectively where: $r = [\text{additive}]/[Zn^{2+}]$, $h = [H_2O]/[Zn^{2+}]$.

In the crystallographic orientation column: diffraction peak indicated in bold corresponds to highly oriented films according to one of three main orientations.

[a] The precursor concentration in the chemical system and thickness are indicated only when they are mentioned in the corresponding reference.

[b] The peaks intensities are very close.

clear colloidal suspension. Matijević [31] reported that the preparation of "monodispersed" sols of metal (hydrous) oxides from metal salts is very sensitive to such factors as salt concentration, nature of the anion, pH, and temperature. He demonstrated that entirely different products result when the anions are changed in the studied systems.

In a previous work [47], we showed the importance of the counter anion in zinc precursors. Hydrated zinc salts (acetate, nitrate, perchlorate) were dissolved in ethanol or 2-methoxyethanol in the presence of monoethanolamine (MEA), which acts at the same time as a base and a complexing agent. Further aging at 60–100 °C, during variable periods, leads to translucent colored colloidal sols or precipitates, according to the counter anion and concentration. For nitrate, no sols could be reproducibly obtained. In perchlorate solutions, excess MEA leads to the formation of sols, after a slow dissolution of the initially formed precipitates. On the contrary, systems stemming from zinc acetate and MEA lead to reproducible systems, under a great variety of experimental conditions. For example, aging at 60 °C for 72 h results in the formation of stable translucent sols by forced hydrolysis of Zn(II) complexes; the necessary water is supplied by the hydrated salt. Acetate plays an important role in sol formation, by complexing Zn(II) cations, in competition with the MEA. The alternative hypotheses for this mechanism will be described in a following section.

After this short comparison of the various precursors used in the sol–gel processes, the use of organic salts as precursors in alcoholic media remains advantageous, on the one hand because of the low cost and the facility of the metal salt use in general, and on the other hand by the fact of avoiding the problems presented by certain inorganic anions and the washing steps.

2.1.2. Solvents

The solvent must present a relatively high dielectric constant in order to dissolve the inorganic salts [52,55,56]. Most alcohols are dipolar, amphiprotic solvents with a dielectric constant that is dependent on the chain length [42]. Table 2 shows the dielectric constants and boiling points of most alcohols used in this work [52,57].

We recall that alcohols with low carbon number, up to 4, are the most used solvents: methanol, ethanol, 1-propanol, 2-propanol, 1-butanol and 2-methoxyethanol (Table 1). In addition, a few works use ethylene glycol ($HOCH_2CH_2OH$) as a solvent that has a dielectric constant of 40.61 (at 25 °C) and a boiling point of 197.4 °C. Among all the monoalcohols, the most used ones are ethanol and 2-propanol. It should be noted that 2-methoxyethanol, despite its good physical properties, is toxic to reproduction, because it is labelled with Risk Phrase R60 (category 2: 'May impair fertility') by the International Programme on Chemical Safety, among others.

Hosono et al. [55], made a comparative study of chemical reactions from zinc acetate dehydrate to ZnO using different types of alcoholic solvents, i.e. methanol, ethanol, and 2-methoxyethanol. Zinc acetate dehydrate (ZAD) was more soluble in methanol than in ethanol or 2-methoxyethanol according to dielectric constants of these alcohols (Table 2). The reflux time necessary for the formation of ZnO increases with the solutions in order, MeOH (12 h) ≪ EtOH (48 h) < 2-ME (72 h). Besides, the same authors demonstrated that the XRD analysis of particles, obtained from the three alcoholic

Table 2
Dielectric constants and boiling points for some alcohols, Refs. [52,57].

Alcohol	Formula	Dielectric constant at 20 °C	Boiling point (°C)
Methanol	CH_3OH	32.35	64.7
Ethanol	CH_3CH_2OH	25.00	78.3
1-Propanol	$CH_3CH_2CH_2OH$	20.81, 20.10 (at 25 °C)	97.2
2-Propanol	$CH_3CH(OH)CH_3$	18.62	82.2
1-Butanol	$CH_3CH_2CH_2CH_2OH$	17.80	117.7
2-Butanol	$CH_3CH_2CH(OH)CH_3$	15.80 (at 25 °C)	99.5
2-Methoxyethanol	$CH_3OCH_2CH_2OH$	16.90	124.6

solutions of ZAD revealed, after refluxing, the formation of intermediate product as $Zn_5(OH)_8(Ac)_2{\cdot}2H_2O$ called layered hydroxide zinc acetate (LHZA). This complex (LHZA) was also observed by Meulenkamp [40] using ethanol as a solvent and by Fujihara et al. [58] or Wang et al. [59] using methanol. On the other hand, Tokumoto et al. [60] have shown by EXAFS and UV spectroscopy that zinc acetate dissolved in ethanol forms zinc oxy-acetate, $Zn_4O(Ac)_6$.

Whichever their nature, these complexes undergo hydrolysis and inorganic polymerization leading to the formation of sols consisting of zinc oxide nanoparticles.

On the other hand, Hosono et al. [55] also showed the washing role and the effect of the reflux time on the cristallinity and the size of particles. It was found that LHZA was removed from the mixture particles, obtained with different reflux times (from 8 to 48 h) in methanolic solution, by washing with MeOH. Both the XRD peak intensities and the crystallite size, determined using the Scherrer's equation, increase monotonically with increasing reflux time, indicating that growth of the ZnO particles proceeds and the crystallinity is improved with time.

2.1.3. Additives

Additives are chemical species presenting at least one functional group, which enables these species to play several roles. They act as basic or acid and/or chelating agent. Alkali metal hydroxides, carboxylic acids, alkanolamines, alkylamines, acetylacetone and polyalcohols are used for this purpose (Table 1). They may facilitate the zinc salt dissolution in some alcoholic media. For example, ZAD has a limited solubility in alcohols like ethanol and 2-propanol in the absence of other agents or heating. The agents, like (mono- to tri-) ethanolamines or lactic acid help in complete dissolution and formation of a stable sol [83]. Furthermore, the additives are believed to play the role of chelating and stabilizing ligands, which avoid the rapid precipitation of zinc hydroxide and allow stable dispersions or solutions to be formed. The amino groups and/or the hydroxyl groups of alkanolamines are known to coordinate the metal atoms of alkoxides, improving the solubility and stability against hydrolysis of the alkoxides [45]. This is also the case with zinc acetate and addition of alkanolamine provides a clear solution. There are two possible ways for MEA a bidentate ligand, to coordinate the zinc atoms; one is to act as a chelating ligand and the other is to bridge two zinc atoms [45]. Among inorganic bases, lithium or sodium hydroxide is often used to form stable dispersions of colloids. Altogether, solvent and additives likely react with zinc cations to give zinc complexes that appear to be the precursor for zinc oxide. Several works have been devoted to the structural characterization of such complexes.

We have proposed in previous work [47,48], described in Section 3.1, another mechanism for the reaction with the main species constituting the precursor solutions (ZAD, ethanol and MEA) when additives such as MEA are employed. In this medium, forced hydrolysis ($[H_2O]/[Zn^{2+}] = 2$) and condensation of the Zn^{2+} cation are relatively slow, due to the low quantities of water (resulting from zinc salt). MEA acts as a complexing agent, also retarding Zn^{2+} condensation; however, the presence of this amine also increases the pH, which should promote the formation of ZnO. The acetate group plays a very relevant role, by complexing Zn^{2+} in competition with the MEA. The complex chemical relationships of the main species are indicated in Scheme 2. In fact, three nucleophilic species (MEA, HO^- and CH_3COO^-) compete for the Zn^{2+} Lewis acid center: attack of an HO^- group leads to the formation of small zinc-oxo-acetate oligomers, which are expected to be formed in the initial stage, from gradual forced hydrolysis of Zn-MEA or Zn-$OCOCH_3$ soluble complexes during aging. The progressive condensation of the hydrolyzed moieties gives rise to colloids or precipitates. Stable acetate-capped colloidal nanometric to sub-micronic particles are likely to be formed in dilute solutions.

2.2. Particle formation

Several works were devoted to the study of the parameters affecting the particle size of zinc oxide. In addition, other works have been devoted to the study of the influence of the precursor and additive concentrations and the solution aging conditions (time and temperature) on the colloids stability and the zinc oxide particles formation (morphology and size). Before this discussion, we recall the possible growth mechanisms proposed by some authors.

2.2.1. Growth mechanisms

Spanhel and Anderson [36] reported that there are two possible ways of describing the growth of ZnO crystals: Ostwald ripening and aggregation. As soon as the smallest stable molecular clusters are formed, they rapidly combine to give the next most stable aggregate. The primary aggregates would further rapidly combine to give the next most stable secondary aggregate and so on. The authors observed that the primary clusters were stable aggregates and would be a result of rapid aggregation rather than a result of Ostwald growth and concluded that the Ostwald mechanism should be considered as only one possible approach to the formation of bulk materials. Meulenkamp [40] suggested also that the particle growth in colloidal systems could be viewed from two standpoints. The first one corresponds to Ostwald ripening: large particles grow at the expense of smaller particles, which have a higher solubility according to the so-called Ostwald–Freundlich equation. This relation is derived from thermodynamic equilibrium considerations and does not, therefore, provide information on the growth rate. The second standpoint describes growth by the addition of reactive precursors available in solution to already existing particles. The rate of particle growth is governed by the concentration of precursors or dissolved species and their reactivity, which depends on the number of particle surface atoms, and the solution composition. Tokumoto et al. [120] reported that the formation of ZnO colloidal particles in an alcoholic solvent consists of two stages. During the early stage of phase transformation, small oligomers are continuously formed. At advanced stages, the aggregation of the oligomers leads to crystalline wurtzite, the primary colloidal particles. The primary particles then aggregate and form a third family, the secondary colloidal particles. The growth of the colloidal particles

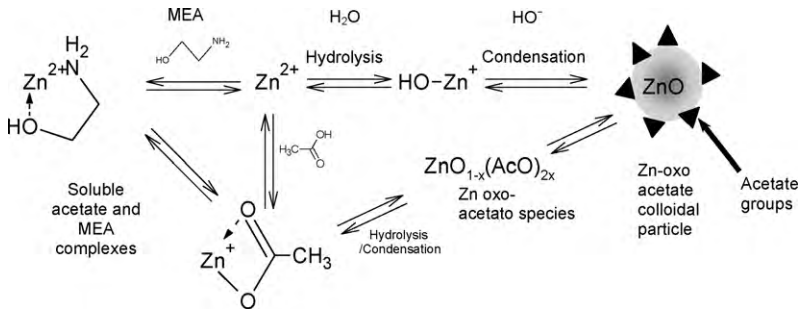

Scheme 2. Sketch of the chemical equilibria taking place in the initial solutions. Hydrolysis and condensation are spurred by temperature. Soluble or colloidal condensed moieties can result, which can be deposited as film precursors; ref. [48].

is a stepped, discontinuous, process indicating that the predominant mechanism of aggregation is heterogeneous coagulation. This mechanism of formation and growth leads to a hierarchical structure.

2.2.2. Nucleation and growth – particle size

Spanhel [121] reported that at least four different "primary particles or clusters" serving as initiators of the ZnO colloid growth, from ZAD as precursor, could be identified to date. The nature of these "primary particles or clusters" depends strongly on the synthesis conditions chosen: initial salt concentration, the temperature and time of the thermal treatment, the nature of alcohol solvent as well as the overall humidity, storage and analysis conditions. Among these primary particles, we can remind $Zn_5(OH)_8(Ac)_2{\cdot}2H_2O$ and $Zn_4O(Ac)_6$, previously discussed in Section 2.1.2 dedicated to solvents.

In other respects, Meulenkamp [40], prepared ZnO nanoparticles by addition of LiOH to an ethanolic zinc acetate solution. He showed that control of the particle size was improved by recognizing the influence of temperature, water, and reaction products during the aging of ZnO sols. Water and acetate induced considerably accelerated particle growth. Hu et al. [42] have synthesized ZnO nanoparticles by precipitation from zinc acetate in a series of n-alkanols from ethanol to 1-hexanol as a function of temperature. The kinetics of nucleation and growth are expected to be strongly dependent on the properties of the solvent. For the shorter chain length alcohols, ethanol and 1-propanol, nucleation and growth are retarded compared to longer chain length alcohols, from 1-butanol to 1-hexanol, where nucleation and growth are fast. The particles size increases with increasing temperature for all solvents and increases with alkanol chain length. In fact, during the growth of colloidal ZnO nanoparticles, the alcohols not only provide the medium for the reactions, but also act as ligands to help to control the morphology and particle size of ZnO [42,56].

2.2.3. Morphology

Chittoffrati and Matijevic [35] clearly showed that the precursor concentration and the aging conditions as well as the nature and the concentration of the additive have an important effect on the morphology of zinc oxide particles. Zinc oxide dispersions were obtained by mixing at room temperature zinc nitrate or sulphate with different bases NaOH or KOH, NH_4OH, triethanolamine or ethylenediamine and cationic or anionic surfactants with varied concentrations, followed by aging for different periods of time at constant elevated temperatures. The authors have demonstrated that precipitates, formed by aging zinc nitrate solutions at elevated temperatures, always consisted of zincite, ZnO, but that the shape and the size of the particles were strongly dependent on the concentration and nature of the reactants. As a rule, particles uniform in shape (and in some cases in size) were obtained only under a certain range of concentrations of the reacting compounds. For example, for the system $Zn(NO_3)_2$–NH_4OH turbidity appeared at room temperature, just after mixing, if $[Zn(NO_3)_2] \geq 3.2 \times 10^{-4}$ mol L^{-1} and $[NH_4OH] \geq 1.0 \times 10^{-3}$ mol L^{-1}. At much lower concentrations of zinc nitrate and ammonia, no precipitation could be detected on mixing the solution at room temperature. On the other hand by heating the diluted solution to 90 °C, reasonably uniform ellipsoidal particles were obtained in small amounts. The particle shape depends also on the concentrations and aging time since intertwined particles were obtained with aging a solution of $[Zn(NO_3)_2] = 5.0 \times 10^{-3}$ mol L^{-1} and $[NH_4OH] = 1.9 \times 10^{-2}$ mol L^{-1} at 90 °C for 3 h, when ellipsoidal particles appeared with $[Zn(NO_3)_2] = 1.0 \times 10^{-4}$ mol L^{-1} and $[NH_4OH] = 3.2 \times 10^{-4}$ mol L^{-1} aged at 90 °C for 1 h. For the other systems and in different concentrations and aging conditions, the particle shapes were: also intertwined particles for $Zn(NO_3)_2$–ethylenediamine, compact spheroidal or ellipsoidal particles for $Zn(NO_3)_2$–triethanolamine and rod-like particles for $Zn(NO_3)_2$–KOH. Substituting $ZnSO_4$ for $Zn(NO_3)_2$ yielded polydispersed platelets in the case of $Zn(NO_3)_2$–triethanolamine system. The concentration domain yielding uniform dispersions depended on the nature of the base employed. Indeed it appeared that the stronger the Zn-base complex, the lower were the concentrations required to generate well-defined particles. Using, in this work, anionic (sodium dodecyl sulphate and a fluorinated polyether) and cationic (cetyltrimethylammonium bromide) surfactants showed that the particle size and aggregation could be affected by the addition of anionic ones.

2.2.4. Colloids stability and thermal behavior

The procedure for ZnO colloids synthesis, first developed by Spanhel and Anderson [36], consists of two major steps: (1) preparing the precursor by reacting zinc acetate with ethanol and (2) hydrolyzing the precursor to form the colloids by using lithium hydroxide. Sakohara et al. [38], using this method, studied the concentration effect of zinc acetate (ZnAc) and lithium hydroxide on the colloids stability as well as their behavior during the thermal analysis. The stability of ZnO colloids was observed to depend on the concentration ratio, ZnAc/LiOH. The prepared colloids with a high ratio (e.g., ZnAc/LiOH = 0.1 M/0.025 M) were quite stable and maintained transparency for more than a month, while a low ratio (e.g., ZnAc/LiOH = 0.025 M/0.025 M) leads to a precipitate within 2 days. For the thermal analysis of ZnO particles, a weight loss was observed from about 200 °C with high ratios (e.g., ZnAc/LiOH = 0.1 M/0.0125 M) but only from 300 °C for low ratios (e.g., ZnAc/LiOH = 0.0125 M/0.025 M). The acetate groups act so to stabilize colloids and this result was also found by Bahnemann et al. [33] and Yang et al. [122].

Sun et al. [56] studied purification and stabilization of colloidal ZnO nanoparticles synthesized from ZAD and potassium hydroxide in methanol. They compared the stability of the purified ZnO nanoparticles redispersed in methanol and in methanol/hexane

solutions at two different volume ratios (7/1 and 3/1). The redispersed purified ZnO nanoparticles were unstable in methanol alone because they become aggregated within several minutes at room temperature. In the case of the redispersion of ZnO nanoparticles in the mixture of methanol/hexane solutions, ZnO nanoparticles would begin to agglomerate at room temperature after a couple of hours and 1 day for the mixtures with a volume ratio 7/1 and 3/1, respectively. So, hexane can stabilize the purified ZnO nanoparticles in methanol and it was also demonstrated that the higher concentration of hexane in the solution, the more stable the solution becomes. The same authors reported that a possible reason why hexane can stabilize the purified ZnO nanoparticles in methanol could be that a small amount of organic non-solvent, i.e., hexane, dissolved in methanol helps to reduce the polarity of the solvent around the acetate-containing ZnO nanoparticle surfaces, thus isolating the ZnO nanoparticles from each other and preventing them from aggregating.

3. Formation of oriented film

3.1. Film formation

In general, films are prepared by dip- or spin-coating of substrate from solutions or sols freshly prepared or aged at room temperature or around 60 °C. The heat treatment of the deposited films is carried out in two steps in most instances as summarized in Table 1, or in one step. For the first step, a pre-heat treatment (40–500 °C) is applied during a short time for solvent evaporation and organic compounds removal [3,4,6,44,46–48,61,62,72,74–76,82–84,86–88,91,92,94,98–100,102,103,111,112,114,123–125]. The second step, a post-heat treatment is employed in order to obtain a well-crystallized films and the final decomposition of organic by-products varying from 250 to 900 °C, according to the substrate nature among others, for all summarized works in Table 1.

The following examples of ZnO thin film elaboration are given for illustration [47,48]. In these works, two approaches were explored to produce *dense films* (method A) or *colloid-based films* (method B).

In the direct *dense film* formation (method A): ZAD was dissolved in a 2-methoxyethanol-MEA solution. The *r* ratio ([MEA]/[$Zn^{(II)}$]) was fixed at 1 or 2, and the final concentration of ZAD was fixed at 0.75 mol L^{-1}. The resultant mixture was allowed to stand at 60 °C for 120 min under stirring leading to a clear and colorless solution, which remained stable for several days. Freshly prepared solution was then deposited on silica glass by spin-coating at 3000 rpm (30 s). These films were pre-heated at 300 °C for 10 min after each coating and this procedure was repeated up to six times. The films were post-heated at 550 °C (1–2 h) in order to obtain crystallized ZnO in wurtzite structure.

For the *colloid-based films* (method B): A 0.2 mol L^{-1} solution of Zn(II) was prepared by refluxing ZAD for 3 h at 80 °C in dry ethanol. MEA and ethanol were subsequently added to adjust the final concentration (0.05 mol L^{-1} of Zn^{2+}) and the solutions were then aged at different temperatures (25–100 °C, in closed vessels) during variable periods (10–240 h). Depending on the [Zn^{2+}] and the *r* ratio ([MEA]/[Zn^{2+}]), transparent solutions or colored colloidal dispersions (bluish to yellow) are obtained. The solution aged at 60 °C for 72 h, leads to a translucent yellow colored sol (colloidal dispersion). The precursor sol was then filtered (Millipore cellulose membranes, 0.45 μm) and deposited on glass substrates by spin-coating (3000 rpm; 30 s). These films were dried (100 °C, 5 min) between successive spin-coating steps. Subsequently, they were pre-treated at 135 °C for 36–72 h, and further post-treated at 450–550 °C for 2 h.

3.2. Main orientations observed

3.2.1. General consideration

The thermodynamically stable crystal structure of ZnO is wurtzite and it occurs in nature as the mineral zincite. Such an ionic and polar structure can be described as a hexagonal close packing (*hcp*) of oxygen and zinc atoms in tetrahedral sites with the space group $C_{6v}^4 = p6_3mc$ [126,127]. The unit cell (a = 3.249 Å, c = 5.205 Å) contains two formula units and the typical crystal habit exhibits two types of low-index surfaces: polar surfaces (0 0 $\bar{1}$) ψ(O terminated) and (0 0 1) ψ(Zn terminated) and non-polar surfaces (1 0 0); and C_{6v} symmetric ones parallel to the *c*-axis [126]. In addition, there is no centre of inversion in the wurtzite structure and therefore an inherent asymmetry is present, which allows anisotropic growth along the *c*-axis. Thus, as has been demonstrated by Li et al. [127] (0 0 2) orientation presents the fastest growth velocity.

Fujihara et al. [102] reported, by studying the sol–gel ZnO thin films, that the orientation is essentially a matter of nucleation and crystal growth and should be explained by the influence of the substrates regardless of epitaxial or non-epitaxial growth. They proposed two possible mechanisms for the orientation of the films on the glass substrates: an initial orientation due to nucleation and a final growth orientation, both of which result from the nucleation at the film/substrate interface. The initial orientation is favored on smooth surfaces with the tendency of nuclei to develop a minimum free energy configuration. The final growth orientation results from survival of nuclei having an energetically unstable plane parallel to the substrate surface among randomly oriented nuclei because of their different growth rates. Comparing with vapor-phase deposition, the authors suggested that the sol–gel process is characterized by the post-deposition crystallization. The films are already supplied with the materials as the amorphous precursors on the substrates before crystallization. Therefore, a driving force for the nucleation is related to reduction of free energy due to transformation from the metastable amorphous to crystalline state in equilibrium. In order for the nucleation to occur preferentially at the substrate surface, the activation energy must be lowered at the film/substrate interface. The same authors [102] studied the thermodynamics of nucleation and crystal growth taking into account the surface energies of the film and the glass substrate and the interfacial energy between them. They reported that the probable mechanisms underlying the *c*-axis orientation are the initial orientation due to nucleation and the final growth orientation at the film/substrate interface and the successive growth in the direction perpendicular to the substrate.

We will present here the crystallographic orientation of films along the main X-ray diffraction peaks of ZnO, which are (1 0 0), (0 0 2) and (1 0 1). Table 1 shows three cases: films fully oriented along (0 0 2) or (1 0 0) and highly oriented films (diffraction peak indicated in bold) according to one of three main orientations. From this table, it appears that all the parameters discussed above play a role on the film orientation. Unfortunately, no clear correlation does exist between each of these parameters and such crystallographic orientation. Thus, only the main tendencies will be underlined hereafter.

3.2.2. Role of the chemical system: precursor nature and its concentration, solvent, additive, aging time

Ohya et al. [44] reported, by comparing ZnO films synthesized from ZAD and zinc n-propoxide as precursors, that the relative intensities in the XRD peaks depend on the precursor nature. They found that the both films showed the three main orientations but that the film derived of zinc acetate exhibited a strong orientation of the *c*-axis.

Kim et al. [3] synthesized ZnO thin films from ZAD/isopropanol/MEA solution with different ZAD concentrations (from 0.3 to

1.3 mol L^{-1}). The coating was performed within 24 h after the solution was prepared and the films were prepared by spin-coating on glass (Corning Inc. 7059) substrate, which was rotated at 3000 rpm. All the films were pre-heated at 250 °C (10 min) and post-heated at 650 °C (1 h). ZnO film as prepared showed very weak XRD peaks when Zn concentration is below the 0.5 mol L^{-1}. For 0.7 mol L^{-1} as a sol concentration, a highly *c*-axis oriented (0 0 2) peak and two weak (1 0 0) and (1 0 1) peaks were observed. Above 1.0 mol L^{-1}, the (0 0 2) peak decreases with increasing Zn concentration, while the (1 0 0) and (1 0 1) peaks gradually increased. O'Brien et al. [79] and Rao et al. [80] studied also the effect of concentration precursor (from 0.3 to 1.3 mol L^{-1}) on the structure of ZnO films, using exactly the same chemical system employed by the previous authors. ZnO thin films were deposited by spin-coating the aged solution (24 h) onto UV fused silica (Spectrosil 2000) glass at rotation speeds of 2000 rpm. The coated substrates were dried on a hotplate at 60 °C (1 h) and annealed at 650 °C (1 h). Only differences in the synthesis method visible in these works [3,79,80] were the substrate nature, the spin-coating speed and the pre-heat treatment temperature but the XRD results were different. So, it was found in these last works [79,80] that all films were polycrystalline and (1 0 0), (0 0 2) and (1 0 1) XRD peaks were observed. The degree of *c*-axis orientation of the ZnO thin films was strongly dependant on the initial zinc concentration and decreased when the concentration increased from 0.3 to 1.3 mol L^{-1}. Films were preferentially oriented in the *c*-axis, or (0 0 2) plane, for zinc concentrations in the range of 0.3–0.6 mol L^{-1}. An increase in zinc concentration to 1.3 mol L^{-1} resulted in a film preferentially oriented in the (1 0 1) plane.

On the other hand, precursor concentration and aging time could play an important role in controlling the competition between the two orientations: *a*-axis (1 0 0) and *c*-axis (0 0 2). Despite that (0 0 2) orientation is the more kinetically favored one; the (1 0 0) one can be observed. Table 1 shows two systems where *a*-axis orientation is obtained and the conditions to induce this orientation could be long aging time and low precursor concentration. The first system, used by Wang et al. [72], is ethanol–acetic acid–water–ZAD (0.19 mol L^{-1}): in this case preferential orientation (1 0 0) has been observed when the sols are aged for 24 h whereas the film appears amorphous for an aging time of 2 h. Since the preparation method and heat treatment of the two films are identical except for the different aging times for the precursor solution at room temperature, the authors [72] reported that such a difference in orientation is attributable to the different nature of the precursor solutions.

In the second system, constituted of ethanol–MEA–ZAD [47,48], of which the process was described in a preceding section, the different preferential orientation of the ZnO films seems to be related to the solution or sol concentration, and the effective coverage of the substrate surface, rather than to the nature of the precursor (i.e. colloidal vs. soluble precursors). Continuous films made up from clear and concentrated solutions ($[Zn^{2+}] = 0.75$ mol L^{-1}) yield (0 0 2) orientation (Figs. 1C, 2A and B). The same is true when using concentrated colloidal sols ($[Zn^{2+}] > 0.2$ mol L^{-1}) as precursors. On the contrary, the (1 0 0) orientation is only obtained when dilute colloidal sols (0.05 mol L^{-1}), aged for 72 h at 60 °C, are used leading to isolated particles (Figs. 1B, 2C and D).

The contact between particles is a critical issue concerning orientation. It is widely recognized that *interaction with the substrate* (and the compatibility of the film and the substrate) plays indeed an important role in nucleation and in the first growth stage, even if for amorphous glass substrates, no epitaxial growth is expected. On the other hand, it is well known that in the growth of thicker films, *the stronger interaction is between the growing particles*; in these conditions growth processes, rather than nucleation, can control the orientation.

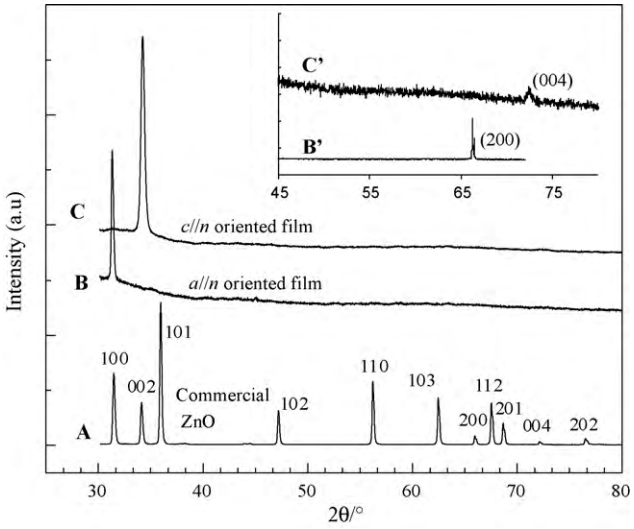

Fig. 1. XRD patterns of commercial zincite reference (A), and ZnO oriented films. (B) *a*//*n* orientation, obtained from a 0.05 mol L^{-1} sol, $h = 2$, 72 h aging at 60 °C and thermal treatment. (C) *c*//*n* orientation, obtained from a 0.75 mol L^{-1} solution, $h = 2$ and thermal treatment. Inset: zoom views of the B and C diffractograms in the 45–80° 2θ range, (B′ and C′, respectively); ref. [48].

As described above, ZnO wurtzite presents basal *polar* oxide or zinc (0 0 1) planes, which are metastable (and thus, present a fast growth rate); the *non-polar* (1 0 0) faces are electrically neutral (Scheme 3A), and present a higher stability [48,128]. Scheme 3 shows the unit cell of ZnO indicating one polar (0 0 1) plane and one non-polar ($0\bar{1}0$) plane (part A); and the scheme of the oriented crystal growth model proposed (part B). We have proposed [48] a very simple analysis, based on the *particle-substrate* versus *particle–particle* interactions, which could explain the different orientations observed in our cases (*a*-axis and *c*-axis), irrespective of the precursor size. This is based on the rearrangements that must take place in the evolution from the as-deposited amorphous material (Zn-oxoacetate) to a crystallized phase. The easiest case to analyze corresponds to the dilute coatings (Figs. 1B, 2C and D). Amorphous spheroidal particles are deposited and submitted to thermal treatment. Upon thermal treatment, the matching between the amorphous silica and the non-polar (1 0 0) face should be better than the matching between any of the polar faces and the substrate. Therefore, the development of a (1 0 0) face on top of the substrate should be energetically more favorable ($\sigma_{ZnO(1\,0\,0)/SiO_2(am)} > \sigma_{ZnO(0\,0\,1)/SiO_2(am)}$), leading to the observed *a*-axis orientation. In the case of a continuous film, originated from the deposition of a gel-like layer, the initially formed Zn-oxoacetate particles are in contact. Here, the particle–particle interactions take over the particle–substrate matching ($\sigma_{ZnO(1\,0\,0)/ZnO(1\,0\,0)}$ should be stronger than $\sigma_{ZnO(1\,0\,0)/SiO_2(am)}$), and *c*-oriented growth dominates, aided by the tendency of the polar planes to develop (Scheme 3B).

We can also underline that when the same chemical system is used (ZAD/ethanol/MEA) and with the same aging time of the solution (72 h) but with a more high precursor concentration (1.8 mol L^{-1}), *a*-axis orientation is not observed and it is rather a film structure showing the three main peaks with a preferential orientation along *c*-axis [71]. The examination of Table 1 shows that there is no synthesis, which gave *a*-axis orientation when the precursor concentration is superior to 0.2 mol L^{-1}.

Ohyama et al. [45] reported that the crystal growth along a preferential direction does not occur by using a solvent that has a low boiling temperature. Solvents with low boiling points disturb the aligned grain growth in the film. Takahashi et al. [44,88] observed preferential orientation of the *c*-axis perpendicular to

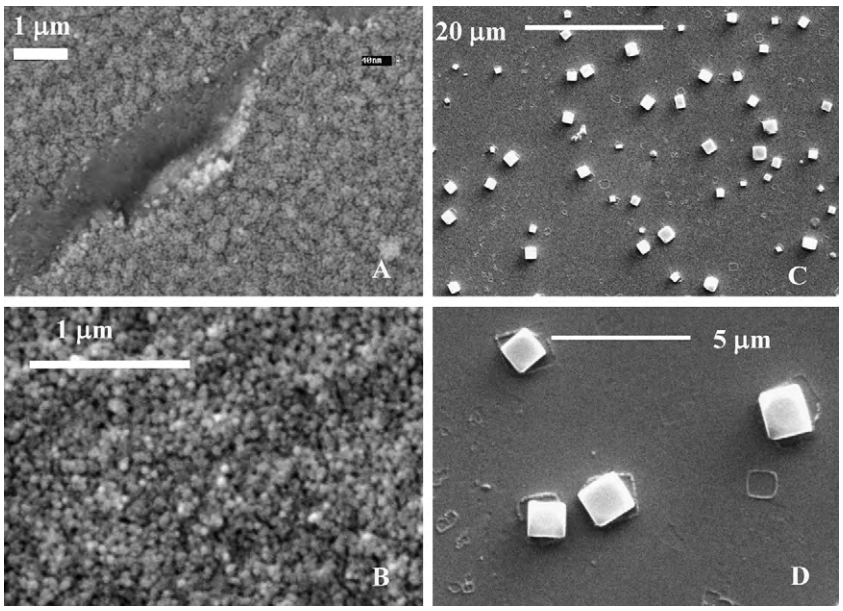

Fig. 2. SEM images of zinc oxide films. (A) Continuous film formed by six ZnO layers (in conditions corresponding to the XRD pattern of Fig. 1C); the intentional crack permits to estimate the thickness. (B) Calcined three-layer films composed by spheroidal ZnO particles. (C) ZnO square slabs, corresponding to the sample shown in Fig. 1B. (D) enlarged view; ref. [48].

the substrate in the sol–gel ZnO films derived from a solution of zinc acetate, 2-propanol and DEA. The preferential orientation was imperfect suggesting that 2-propanol, a solvent with low boiling point, hinders strongly preferential orientation. In contrast, the use of solvents with higher boiling points, like 2-methoxyethanol and MEA, resulted in strongly preferential orientation of ZnO crystals as demonstrated by Ohyama et al. [45]. These authors suggested, as an explanation of the effect of the solvent boiling point for ZnO crystallization, that a solvent of higher boiling point would evaporate more slowly on heating, allowing the structural relaxation of the gel film before crystallization. We observed the same effect of the alcohol nature on the crystallographic orientation of ZnO thin films. Indeed, XRD patterns of the films obtained from ethanol (boiling point: 78.3 °C) showed the three main peaks while those of the derived films of 2-methoxyethanol (boiling point: 124.6 °C) correspond to highly *c*-axis oriented films, using the same ZAD concentration (0.75 mol L^{-1}) and MEA ratio of 2 in the both cases [47].

The preferential orientation is also considered to be due to differences in the zinc coordination power and the boiling points of the additives, as was demonstrated by Nishio et al. [129]. The authors have compared the effect of diethanolamine (DEA), diethylenetriamine, MEA and acetylacetone on the *c*-axis orientation, using ethanol as solvent. The boiling points of these additives are 271 °C for DEA, 207.1 °C for diethylenetriamine, 171.1 °C for MEA and 140 °C for acetylacetone [129]. The authors found that the films, prepared with acetylacetone and MEA, are highly *c*-axis oriented in contrast with the others films from DEA and diethylenetriamine. Ohyama et al. [45] compared ZnO films obtained from two solutions containing different additives: MEA and DEA. XRD results showed that the films obtained with MEA and annealed between 400 and 600 °C, were highly oriented along *c*-axis. On the other hand, using DEA as additive leads to ZnO films showing the three XRD peaks and with a very weak intensity for the same heat treatment temperature range. The authors suggested that this difference is probably due to the structure of alkanolamine-zinc acetate complexes, formed in the solutions, which could be different between MEA and DEA because DEA is a terdentate ligand and MEA a bidentate ligand. Also, Yoon et al. [106] compared the effect of the additive nature (MEA and DEA) on the film structure and using two different substrates (SiN_x/Si and Pt(1 1 1)/Si). They found that the films obtained with MEA showed only a very intense XRD (0 0 2) peak independently of the substrate nature. On the contrary, DEA leads to a very weak XRD (0 0 2) peak only with Pt(1 1 1)/Si and not with SiN_x/Si as a substrate.

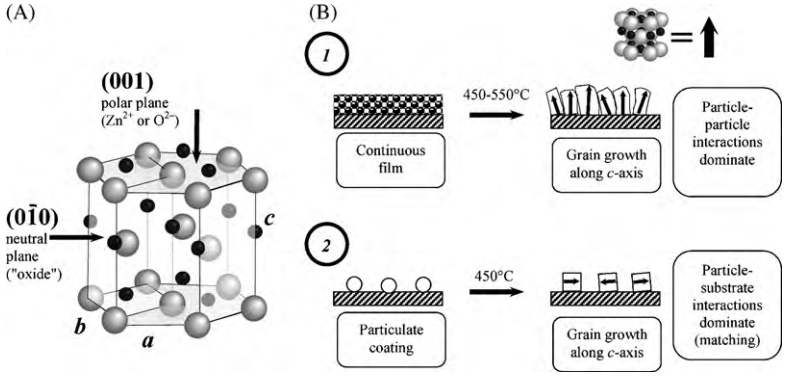

Scheme 3. (A) Unit cell of ZnO, indicating one polar (0 0 1) plane, and one non-polar (0 $\bar{1}$ 0) plane. Zn^{2+} cations are represented in black, O^{2-} anions in grey. (B) Scheme of the oriented crystal growth model proposed. While grain growth is always along the *c*-axis; the orientation depends on the type of interactions that dominate. In both cases, the "matching" of the non-polar ("oxide-like") planes is a determinant factor of orientation; ref. [48].

On the other hand, Sagar et al. [65] studied the effect of the sol pH increasing by MEA addition, to ZAD methanolic solution, on the microstructure of ZnO thin films. They reported that the pH of modified sols was found to increase continuously from 6.4 to 10.6 with increase in value of the ratio of additive MEA to ZAD precursor (r) from 0 to 1, respectively. This increase is attributed to hydrolysis of salts of weak acid in strong base medium. The XRD pattern of ZnO thin films deposited on corning glass, with sols having different ratio of MEA (r) and annealed at 600 °C, showed preferred c-axis orientation and the intensity of (0 0 2) peak was found to increase with increase in r ratio from 0 to 1. The increase in (0 0 2) peak intensity is an indication of the large amount of volume of crystallites oriented along (0 0 2) plane and clearly indicate that the addition of MEA in sols improve the crystalline nature of deposited ZnO film. We reported that the higher alkaline nature of sols is to be useful in enhancing the formation of ZnO crystallites [48]. Also, we demonstrated that the MEA ratio (r) has an influence on the preferential orientation when r-value of 2 leads to highly c-axis oriented films while the three XRD peaks are observed with r-value of 1, using the same ZAD concentration (0.75 mol L^{-1}) and the same alcohol (2-methoxyethanol) in the both cases [47].

Finally, it should be noted that a few works have also observed the rare (1 0 0) orientation. According to these works, the main reasons leading to such a (1 0 0) orientation are (i) epitaxial growth, or (ii) preferential adsorption of molecules such as tetrasulfonated metallophtalocyanine on the (0 0 2) face of ZnO elaborated by electrodeposition [130].

3.2.3. Role of coating: method, speed, thickness, substrate

ZnO films are elaborated by either spin and/or dip-coatings. For the works summarized in Table 1, only one paper shows comparison between the two coating methods and the effect on ZnO films structure. So, Habibi and Sardashti [131] reported that the crystallographic orientation of ZnO films depends also on the coating method. They observed a highly c-axis oriented films with dip-coating method (withdrawal speed of 1 cm/min) while XRD patterns of films deposited by spin-coating (3000 rpm) showed the three peaks with high intensity for (0 0 2) peak. The peaks intensities increase when the post-heat treatment increases from 350 to 550 °C (1 h). The both films were prepared with the same other parameters: ZAD/isopropanol/MEA as chemical system, glass substrate, pre-heat treatment of 275 °C (10 min) and five deposited layers.

Ohyama et al. [98] synthesized ZnO films using dip-coating and with three different withdrawal speed (1.2, 3.5 and 7 cm/min). They have observed that a low withdrawal speed (WS) resulted in denser post-heated films. When the WS is low, the film thickness per one dipping is small, and the solvent can more easily evaporate from the film. This can cause the larger shrinkage of the film, giving denser gel films. A higher preferred (0 0 2) orientation was found for the films prepared with lower WD's (1.2 cm/min). The authors proposed two possible interpretations: (i) since preferential orientation can occur via nucleation at the film/substrate interface, it is feasible that unidirectional growth of ZnO crystals can more proceed in a dense matrix than in a porous one, and (ii) the solvent and the organic substances produced by thermal decomposition can evaporate more easily out of thinner film without disturbing the oriented crystal growth.

The thickness is also a parameter, which has a role on the degree of crystal orientation. It is closely related to some of the other parameters. So, it increases when the number of coatings [86,129,132] and the precursor concentration [79,87,90] increase, and it decreases when the spin-coating speed [87] and the post-heat treatment [73,84,114] increase. It also increases almost linearly with withdrawal speed in the case of dip-coating. It is expected that the XRD peaks intensities should increase in proportion to the film thickness. Furthermore Aslan et al. [82] and Habibi and Sardashti [133] have shown that preferential orientation along the c-axis slightly increased as the film thickness or the number of coatings increased.

On the other hand, Ohyama et al. [98] and Mridha and Basak [89] established that there exists a critical thickness above which well (0 0 2) oriented films are obtained. In fact, by varying the number of coating from 1 to 5, Ohyama et al. [98] reported that the relative intensity of (0 0 2) peak was not proportional to the film thickness below 100 nm (three coatings), and particularly the peak intensity of ZnO film with one dip-coating was very weak. The relative intensity of (0 0 2) peak increases abruptly with increasing film thickness from 50 to 100 nm (1–3 coatings) and then increases gradually in proportion to film thickness. These imply that the crystal growth at the film/substrate interface is affected by the substrate not to a less extent. When the as-deposited gel film is subjected to pre-heat treatment (300 °C), the nucleation of ZnO occurs at the film/substrate interface. However, the glass substrate probably disturbs the oriented crystal growth because of the random atomic arrangement of the substrate. Consequently, the peak intensity of (0 0 2) plane was very weak. On the other hand, the oriented grain growth in the second layer may easily occur because of the presence of slightly oriented grains. Then, the peak intensity of (0 0 2) plane increases abruptly. Mridha and Basak [89] studying also the effect of thickness on the structural properties of ZnO films, they varied the number of spin-coatings, on glass substrate, in order to obtain different thicknesses (from 55 to 600 nm). The XRD results indicated that all the films were polycrystalline and randomly oriented, and the relative intensities of the three main peaks were dependents on the film thickness. The authors suggested that although Ohyama et al. [45,98] and Natsume and Sakata [61] reported c-axis oriented ZnO films on glass substrates, the random orientation in their films was probably due to the difference in the precursor chemistry and heat treatment temperatures as also reported by Fujihara et al. [102]. On the other hand, they found that as the film thickness was increased, (0 0 2) orientation was preferred and became maximum for the film of thickness 260 nm indicating that the crystalline quality of the film gets better as the film grows thicker. Above this thickness, the film again becomes randomly oriented.

Concerning the substrates, there are two kinds: crystalline and amorphous ones. As already well established, the use of well-crystallized substrates can help to obtain a desired orientation of the film. This is particularly true when the substrate cell unit matches very well that of deposed compound. This is the case when ZnO film is deposed on a silicon substrate whose a cubic parameter is very close to the c parameter of the hexagonal cell of ZnO.

The examination of Table 1 shows, however, that amorphous substrates generally lead to oriented zinc oxide films along the (0 0 2) direction. This point has clearly been discussed by Chakrabarti et al. [83]. Indeed, these authors obtained oriented (0 0 2) film when a glass substrate is used whereas crystalline substrates such as quartz and silicon lead to less oriented films. This difference has been attributed to non-bridging oxygens (NBO's), which help the (0 0 2) growth of zinc oxide. Conversely, crystalline substrates such as quartz do not present such a required condition since all the oxygen atoms are involved in corner-sharing SiO_4 tetrahedra of the three dimensional network [83].

3.2.4. Role of the heat treatments: pre-heat treatment and post-heat treatment

The heat treatment appears to be one of the most important factors governing the film orientation. As discussed above, the pre-heat treatment appears to be a crucial step. Indeed, it governs the orientation of the crystallites during solvent evaporation and removal of the organic compounds. The temperature of this treat-

ment varies from case to case, but a clear rule can be deduced in its choice. It should be higher than the boiling point of the solvent and the additives and near the crystallization temperature of ZnO. A temperature around 300 °C appears to be the most appropriate [98,112] in the case of 2-methoxyethanol and MEA as solvent and additive, respectively, to produce (0 0 2) oriented films. This temperature has also been observed for the system consisting of methanol and lactic acid [46]. On the contrary, a pre-heat temperature of 100 °C for the films obtained from 2-propanol and DEA was sufficient for observing full (0 0 2) orientation [83]. A similar low pre-heat temperature (80 °C) has also been used for the chemical systems consisting of methanol as solvent without using any additives [61].

Beside the pre-heat treatment, the post-heat temperature should be carefully chosen. The preferential orientation, for instance (0 0 2), increases with increasing temperature. For, a great number of systems, a temperature range of 500–600 °C appears to be the most appropriate one. It should, however, be noted that there exists for each system an upper limit in temperature above which the loss of orientation is observed [98,112].

The pre-heat temperature seems to be the most important factor for obtaining ZnO films with preferred orientation [54,76,98,134], affecting the solvent vaporization, zinc acetate decomposition and zinc oxide crystal growth. Removal of the solvent and organic substances produced by acetate decomposition prior to crystallization may be one of the key factors that provide oriented crystal growth [48,76,98,134].

4. Conclusion

Considerable work has been carried out on the development of ZnO films in view of various applications. Several synthesis methods belonging to the sol–gel route have been developed for this purpose. The major part leads to oriented films along the (0 0 2) direction and there are only a few works showing (1 0 0) orientation. Interestingly, (0 0 2) orientation appears to be favored by amorphous substrates. ZnO crystallites with preferential orientation are desirables for applications where crystallographic anisotropy is a prerequisite e.g. UV diode lasers [9–18], piezoelectric surface acoustic wave or acousto-optic devices [3,5,19–21].

Acknowledgement

The author thanks his colleague Dr. Xavier Bonnin for his precious help.

References

[1] D.C. Look, Mater. Sci. Eng., B 80 (2001) 383–387.
[2] R. Triboulet, J. Perrière, Prog. Cryst. Growth Charact. Mater. 47 (2003) 65–138.
[3] Y.-S. Kim, W.-P. Tai, S.-J. Shu, Thin Solid Films 491 (2005) 153–160.
[4] C. Shaoqiang, Z. Jian, F. Xiao, W. Xiaohua, L. Laiqiang, S. Yanling, X. Qingsong, W. Chang, Z. Jianzhong, Z. Ziqiang, Appl. Surf. Sci. 241 (2005) 384–391.
[5] Z. Ye, G. Yuan, B. Li, L. Zhu, B. Zhao, J. Huang, Mater. Chem. Phys. 93 (2005) 170–173.
[6] R. Ghosh, B. Mallik, S. Fujihara, D. Basak, Chem. Phys. Lett. 403 (2005) 415–419.
[7] T. Makino, C.H. Chia, Nguen T. Tuan, Y. Segawa, M. Kawasaki, A. Ohtomo, K. Tamura, H. Koinuma, Appl. Phys. Lett. 77 (2000) 1632–1634.
[8] D.C. Reynolds, D.C. Look, B. Jogai, Solid State Commun. 99 (1996) 873–875.
[9] P. Zu, Z.K. Tang, G.K.L. Wong, M. Kawasaki, A. Ohtomo, H. Koinuma, Y. Segawa, Solid State Commun. 103 (1997) 459–463.
[10] D.M. Bagnall, Y.F. Chen, Z. Zhu, T. Yao, S. Koyama, M.Y. Shen, T. Goto, Appl. Phys. Lett. 70 (1997) 2230–2232.
[11] Y. Segawa, A. Ohtomo, M. Kawasaki, H. Koinuma, Z.K. Tang, P. Yu, G.K.L. Wong, Phys. Status Solidi B 202 (1997) 669–672.
[12] D.M. Bagnall, Y.F. Chen, M.Y. Shen, Z. Zhu, T. Goto, T. Yao, J. Cryst. Growth 184–185 (1998) 605–609.
[13] P. Yu, Z.K. Tang, G.K.L. Wong, M. Kawasaki, A. Ohtomo, H. Koinuma, Y. Segawa, J. Cryst. Growth 184–185 (1998) 601–604.
[14] Z.K. Tang, G.K.L. Wong, P. Yu, M. Kawasaki, A. Ohtomo, H. Koinuma, Y. Segawa, Appl. Phys. Lett. 72 (1998) 3270–3272.
[15] M. Kawasaki, A. Ohtomo, I. Ohkubo, H. Koinuma, Z.K. Tang, P. Yu, G.K.L. Wong, B.P. Zhang, Y. Segawa, Mater. Sci. Eng., B 56 (1998) 239–245.
[16] A. Ohtomo, M. Kawasaki, Y. Sakurai, Y. Yoshida, H. Koinuma, P. Yu, Z.K. Tang, G.K.L. Wong, Y. Segawa, Mater. Sci. Eng., B 54 (1998) 24–28.
[17] H. Lin, S. Zhou, T. Huang, H. Teng, X. Liu, S. Gu, S. Zhu, Z. Xie, P. Han, R. Zhang, J. Alloys Compd. 467 (2009) L8–L10.
[18] M. Wraback, H. Shen, S. Liang, C.-R. Gorla, Y. Lu, Appl. Phys. Lett. 74 (1999) 507–509.
[19] D.-M. Schaadt, O. Brandt, S. Ghosh, T. Flissikowski, U. Jahn, H.-T. Grahn, Appl. Phys. Lett. 90 (2007) 231117–231119.
[20] R. Romero, D. Leinen, E.-A. Dalchiele, J.-R. Ramos-Barrado, F. Martín, Thin Solid Films 515 (2006) 1942–1949.
[21] P.-M. Martin, M.-S. Good, J.-W. Johnston, G.-J. Posakony, L.-J. Bond, S.-L. Crawford, Thin Solid Films 379 (2000) 253–258.
[22] R. Ondo-Ndong, F. Delannoy, A. Giani, A. Boyer, A. Foucaran, Mater. Sci. Eng., B 97 (2003) 68–73.
[23] R. Ondo-Ndong, G. Ferblantier, M. Al Khalfioui, A. Boyer, A. Foucaran, J. Cryst. Growth 255 (2003) 130–135.
[24] R. Al Asmar, G. Ferblantier, F. Mailly, A. Foucaran, Phys. Status Solidi C 2 (2005) 1331–1335.
[25] R. Al Asmar, G. Ferblantier, Fredrick Mailly, P. Gall-Borrut, A. Foucaran, Thin Solid Films 473 (2005) 49–53.
[26] S.M. Abrarov, Sh.U. Yuldashev, T.W. Kim, S.B. Lee, H.Y. Kwon, T.W. Kang, J. Lumin. 114 (2005) 118–124.
[27] S.M. Abrarov, Sh.U. Yuldashev, T.W. Kim, S.B. Lee, Y.H. Kwon, T.W. Kang, Opt. Commun. 250 (2005) 111–119.
[28] R. Ayouchi, D. Leinen, F. Martın, M. Gabas, E. Dalchiele, J.R. Ramos-Barrado, Thin Solid Films 426 (2003) 68–77.
[29] T. Pauporteï, D. Lincot, Electrochim. Acta 45 (2000) 3345–3353.
[30] E.-B. Yousfi, J. Fouache, D. Lincot, Appl. Surf. Sci. 153 (2000) 223–234.
[31] E. Matijević, Acc. Chem. Res. 14 (1981) 22–29.
[32] U. Koch, A. Fojtik, H. Weller, A. Henglein, Chem. Phys. Lett. 122 (1985) 507–510.
[33] D.W. Bahnemann, C. Kormann, M.R. Hoffmann, J. Phys. Chem. 91 (1987) 3789–3798.
[34] M. Haase, H. Weller, A. Henglein, J. Phys. Chem. 92 (1988) 482–487.
[35] A. Chittofrati, E. Matijević, Colloids Surf. 48 (1990) 65–78.
[36] L. Spanhel, M.A. Anderson, J. Am. Chem. Soc. 113 (1991) 2826–2833.
[37] P.V. Kamat, B. Patrick, J. Phys. Chem. 96 (1992) 6829–6834.
[38] S. Sakohara, M. Ishida, M.A. Anderson, J. Phys. Chem. B 102 (1998) 10169–10175.
[39] M. Hilgendorff, L. Spanhel, Ch. Rothenhäusler, G. Müller, J. Electrochem. Soc. 145 (1998) 3632–3637.
[40] E.A. Meulenkamp, J. Phys. Chem. B 102 (1998) 5566–5572.
[41] E.M. Wong, J.E. Bonevich, P.C. Searson, J. Phys. Chem. B 102 (1998) 7770–7775.
[42] Z. Hu, G. Oskam, P.C. Searson, J. Colloid Interface Sci. 263 (2003) 454–460.
[43] T. Okamura, Y. Seki, S. Nagakari, H. Okushi, Jpn. J. Appl. Phys. 31 (1992) L762–L764.
[44] Y. Ohya, H. Saiki, Y. Takahashi, J. Mater. Sci. 29 (1994) 4099–4103.
[45] M. Ohyama, H. Kozuka, T. Yoko, S. Sakka, J. Ceram. Soc. Jpn. 104 (1996) 296–300.
[46] D. Bao, H. Gu, A. Kuang, Thin Solid Films 312 (1998) 37–39.
[47] L. Znaidi, G.J.A.A. Soler Illia, R. Le Guennic, C. Sanchez, A. Kanaev, J. Sol–Gel Sci. Technol. 26 (2003) 817–821.
[48] L. Znaidi, G.J.A.A. Soler Illia, S. Benyahia, C. Sanchez, A.V. Kanaev, Thin Solid Films 428 (2003) 257–262.
[49] S. Ben Yahia, L. Znaidi, A. Kanaev, J.P. Petitet, Spectrochim. Acta, Part A 71 (2008) 1234–1238.
[50] (a) J. Livage, D. Ganguli, Sol. Energy Mater. Sol. Cells 68 (2001) 365–381; (b) J. Livage, Curr. Opin. Solid State Mater. Sci. 2 (1997) 132–138.
[51] M. Guglielmi, G. Carturan, J. Non-Cryst. Solids 100 (1988) 16–30.
[52] M.Z.-C. Hu, E.A. Payzant, C.H. Byers, J. Colloid Interface Sci. 222 (2000) 20–36.
[53] A.C. Pierre, Introduction to Sol–Gel Processing, Kluwer Academic Publishers, Boston/Dordrecht/London, 1998, pp. 91–167.
[54] L. Armelao, M. Fabrizio, S. Gialanella, F. Zordan, Thin Solid Films 394 (2001) 90–96.
[55] E. Hosono, S. Fujihara, T. Kimura, H. Imai, J. Sol–Gel Sci. Technol. 29 (2004) 71–79.
[56] D. Sun, M. Wong, L. Sun, Y. Li, N. Miyatake, H.J. Sue, J. Sol–Gel Sci. Technol. 43 (2007) 237–243.
[57] Sigma Aldrich Data: Physical properties of solvents, http://www.sigmaaldrich.com/img/assets/13620/LabBasics_pg144.pdf.
[58] S. Fujihara, E. Hosono, T. Kimura, J. Sol–Gel Sci. Technol. 31 (2004) 165–168.
[59] H. Wang, C. Xie, D. Zeng, J. Cryst. Growth 277 (2005) 372–377.
[60] M.S. Tokumoto, V. Briois, C.V. Santilli, S.H. Pulcinelli, J. Sol–Gel Sci. Technol. 26 (2003) 547–551.
[61] Y. Natsume, H. Sakata, Thin Solid Films 372 (2000) 30–36.
[62] A.E.J. González, J.A.S. Urueta, R.S. Parra, J. Cryst. Growth 192 (1998) 430–438.
[63] A.M.P. Santos, E.J.P. Santos, Thin Solid Films 516 (2008) 6210–6214.
[64] A.M.P. Santos, E.J.P. Santos, Mater. Lett. 61 (2007) 3432–3435.
[65] P. Sagar, P.K. Shishodia, R.M. Mehra, Appl. Surf. Sci. 253 (2007) 5419–5424.
[66] P. Sagara, P.K. Shishodiaa, R.M. Mehra, H. Okadab, A. Wakaharab, A. Yoshida, J. Lumin. 126 (2007) 800–806.
[67] Z. Liu, Z. Jin, W. Li, J. Qiu, Mater. Lett. 59 (2005) 3620–3625.
[68] Z. Liu, J. Li, J. Ya, Y. Xin, Z. Jin, Mater. Lett. 62 (2008) 1190–1193.

[69] M. Wang, E.J. Kim, J.S. Chung, E.W. Shin, S.H. Hahn, K.E. Lee, C. Park, Phys. Status Solidi A 203 (2006) 2418–2425.
[70] N. Kumar, R. Kaur, R.M. Mehra, J. Lumin. 126 (2007) 784–788.
[71] J. Wang, Y. Qi, Z. Zhi, J. Guo, M. Li, Y. Zhang, Smart Mater. Struct. 16 (2007) 2673–2679.
[72] X.H. Wang, J. Shi, S. Dai, Y. Yang, Thin Solid Films 429 (2003) 102–107.
[73] M.P. Bole, D.S. Patil, J. Phys. Chem. Solids 70 (2009) 466–471.
[74] Y. Kavanagh, D.C. Cameron, Thin Solid Films 398–399 (2001) 24–28.
[75] L. Bahadur, T.N. Rao, J. Photochem. Photobiol., A 91 (1995) 233–240.
[76] R. Brenier, L. Ortéga, J. Sol–Gel Sci. Technol. 29 (2004) 137–145.
[77] J. Petersen, C. Brimont, M. Gallart, O. Crégut, G. Schmerber, P. Gilliot, B. Hönerlage, C. Ulhaq-Bouillet, J.L. Rehspringer, C. Leuvrey, S. Colis, A. Slaoui, A. Dinia, Microelectron. J. 40 (2009) 239–241.
[78] D. Raoufi, T. Raoufi, Appl. Surf. Sci. 255 (2009) 5812–5817.
[79] S. O'Brien a, L.H.K. Koh, G.M. Crean, Thin Solid Films 516 (2008) 1391–1395.
[80] J. Rao, R.J. Winfield, L.H.K. Koh, S. O'Brien, G.M. Crean, Phys. Status Solidi A 205 (2008) 1938–1942.
[81] L.Y. Lin, D.E. Kim, Thin Solid Films 517 (2009) 1690–1700.
[82] M.H. Aslan, A.Y. Oral, E. Menşur, A. Gűl, E. Başaran, Sol. Energy Mater. Sol. Cells 82 (2004) 543–552.
[83] S. Chakrabarti, D. Ganguli, S. Chaudhuri, Mater. Lett. 58 (2004) 3952–3957.
[84] Z. Jiwei, Z. Liangying, Y. Xi, Ceram. Int. 26 (2000) 883–885.
[85] M. Wang, J. Wang, W. Chen, Y. Cui, L. Wang, Mater. Chem. Phys. 97 (2006) 219–225.
[86] H.Y. Bae, G.M. Choi, Sens. Actuators, B 55 (1999) 47–54.
[87] Y. Ohya, H. Saiki, T. Tanaka, Y. Takahashi, J. Am. Ceram. Soc. 79 (1996) 825–830.
[88] Y. Takahashi, M. Kanamori, A. Kondoh, H. Minoura, Y. Ohya, Jpn. J. Appl. Phys. 33 (1994) 6611–6615.
[89] S. Mridha, D. Basak, Mater. Res. Bull. 42 (2007) 875–882.
[90] M. Dutta, S. Mridha, D. Basak, Appl. Surf. Sci. 254 (2008) 2743–2747.
[91] D. Basak, G. Amin, B. Mallick, G.K. Paul, S.K. Sen, J. Cryst. Growth 256 (2003) 73–77.
[92] R. Ghosh, D. Basak, S. Fujihara, J. Appl. Phys. 96 (2004) 2689–2692.
[93] R. Ghosh, S. Fujihara, D. Basak, J. Electron. Mater. 35 (2006) 1728–1733.
[94] Y. Zhang, B. Lin, X. Sun, Z. Fu, Appl. Phys. Lett. 86 (2005) 131910/1–131910/3.
[95] B. Pal, M. Sharon, Mater. Chem. Phys. 76 (2002) 82–87.
[96] A. Abdel Aal, S.A. Mahmoud, A.K. Aboul-Gheit, Nanoscale Res. Lett. 4 (2009) 627–634.
[97] Y. Caglar, S. Ilican, M. Caglar, F. Yakuphanoglu, J. Wu, K. Gao, P. Lu, D. Xue, J. Alloys Compd. 481 (2009) 885–889.
[98] M. Ohyama, H. Kozuka, T. Yoko, Thin Solid Films 306 (1997) 78–85.
[99] H. Li, J. Wang, H. Liu, H. Zhang, X. Li, J. Cryst. Growth 275 (2005) e943–e946.
[100] H. Li, J. Wang, H. Liu, C. Yang, H. Xu, X. Li, H. Cui, Vacuum 77 (2004) 57–62.
[101] M.W. Zhu, J.H. Xia, R.J. Hong, H. Abu-Samra, H. Huang, T. Staedler, J. Gong, C. Sun, X. Jiang, J. Cryst. Growth 310 (2008) 816–823.
[102] S. Fujihara, C. Sasaki, T. Kimura, Appl. Surf. Sci. 180 (2001) 341–350.
[103] T. Nagase, T. Ooie, J. Sakakibara, Thin Solid Films 357 (1999) 151–158.
[104] P.T. Hsieh, Y.C. Chen, K.S. Kao, M.S. Lee, C.C. Cheng, J. Eur. Ceram. Soc. 27 (2007) 3815–3818.
[105] P.T. Hsieh, Y.C. Chen, M.S. Lee, K.S. Kao, M.C. Kao, M.P. Houng, J. Sol–Gel Sci. Technol. 47 (2008) 1–6.
[106] S.H. Yoon, D. Liu, D. Shen, M. Park, D.J. Kim, J. Mater. Sci. 43 (2008) 6177–6181.
[107] B.K. Choi, D.H. Chang, Y.S. Yoon, S.J. Kang, J. Mater. Sci.: Mater. Electron. 17 (2006) 1011–1015.
[108] G. Srinivasan, J. Kumar, Cryst. Res. Technol. 41 (2006) 893–896.
[109] G. Srinivasan, N. Gopalakrishnan, Y.S. Yu, R. Kesavamoorthy, J. Kumar, Superlattices Microstruct. 43 (2008) 112–119.
[110] G. Srinivasan, R.T. Rajendra Kumar, J. Kumar, J. Sol–Gel Sci. Technol. 43 (2007) 171–177.
[111] Y. Kokubun, H. Kimura, S. Nakagomi, Jpn. J. Appl. Phys. 42 (2003) L904–L906.
[112] J.H. Lee, K.-H. Ko, B.-O. Park, J. Cryst. Growth 247 (2003) 119–125.
[113] S.W. Xue, X.T. Zu, L.X. Shao, Z.L. Yuan, W.G. Zheng, X.D. Jiang, H. Deng, J. Alloys Compd. 458 (2008) 569–573.
[114] R. Castanedo-Pérez, O. Jiménez-Sandoval, S. Jiménez-Sandoval, J. Márquez-Marín, A. Mendoza-Galván, G. Torres-Delgado, A. Maldonado-Alvarez, J. Vac. Sci. Technol. A 17 (1999) 1811–1816.
[115] G. Torres Delgado, C.I. Zúñiga Romero, S.A. Mayén Hernández, R. Castanedo-Pérez, O. Zelaya Angel, Sol. Energy Mater. Sol. Cells 93 (2009) 55–59.
[116] M.N. Kamalasanan, S. Chandra, Thin Solid Films 288 (1996) 112–115.
[117] A. Chatterjee, C.H. Shen, A. Ganguly, L.C. Chen, C.W. Hsu, J.Y. Hwang, K.H. Chen, Chem. Phys. Lett. 391 (2004) 278–282.
[118] M. Toyoda, J. Watanabe, T. Matsumiya, J. Sol–Gel Sci. Technol. 1–2 (1999) 93–99.
[119] T. Okamura, Y. Seki, S. Nagakari, H. Okushi, Jpn. J. Appl. Phys. 31 (1992) 3218–3220.
[120] M.S. Tokumoto, S.H. Pulcinelli, C.V. Santilli, A.F. Craievich, J. Non-Cryst. Solids 247 (1999) 176–182.
[121] L. Spanhel, J. Sol–Gel Sci. Technol. 39 (2006) 7–24.
[122] R.D. Yang, S. Tripathy, Y. Li, H.-J. Sue, Chem. Phys. Lett. 411 (2005) 150–154.
[123] Y. Natsume, H. Sakata, Mater. Chem. Phys. 78 (2002) 170–176.
[124] N. Asakuma, H. Hirashima, H. Imai, T. Fukui, M. Toki, J. Sol–Gel Sci. Technol. 26 (2003) 181–184.
[125] S. Sakohara, L.D. Tickanen, M.A. Anderson, J. Phys. Chem. 96 (1992) 11086–11091.
[126] J.H. Guo, L. Vayssieres, C. Persson, R. Ahuja, B. Johansson, J. Nordgren, J. Phys.: Condens. Matter. 17 (2005) 235–240.
[127] W.J. Li, E.W. Shi, W.Z. Zhong, Z.W. Yin, J. Cryst. Growth 203 (1999) 186–196.
[128] L. Vayssieres, K. Keis, A. Hagfeldt, S.-E. Lindquist, Chem. Mater. 13 (2001) 4395–4398.
[129] K. Nishio, S. Miyake, T. Sei, Y. Watanabe, T. Tsuchia, J. Mater. Sci. 31 (1996) 3651–3656.
[130] T. Yoshida, M. Tochimoto, D. Schlettwein, D. Wöhrle, T. Sugiura, H. Minoura, Chem. Mater. 11 (1999) 2657–2667.
[131] M.H. Habibi, M.K. Sardashti, J. Iran. Chem. Soc. 5 (2008) 603–609.
[132] L. Znaidi, S. Benyahia, C. Marchand, J.P. Gaston, J. Kurdi, J.F. Guillemoles, Nineteenth European Photovoltaic Solar Energy Conference Proceedings of the international Conference held in Paris, France, 7–11 June, 2004, pp. 301–304.
[133] M.H. Habibi, M.K. Sardashti, J. Nanomater. (2008) 1–5.
[134] C. Lu, J.Y. Cho, H.J. Chang, S.W. Joo, Y. Wang, Mater. Sci. Forum 449–452 (2004) 1009–1012.